Astronomy & Astrophysics manuscript no. patternz
February 10, 2012

Bar pattern speed evolution over the last 7 Gyr

I. Pérez,[1,2] J.A.L. Aguerri[3,4] and J. Méndez-Abreu[3,4]

[1] Dpto. de Física Teórica y del Cosmos, University of Granada, Facultad de Ciencias (Edificio Mecenas), 18071-Granada, Spain
e-mail: isa@ugr.es
[2] Instituto Carlos I de Física Teórica y Computación
[3] Instituto de Astrofísica de Canarias, C/ Vía Láctea s/n, 38200 La Laguna, Spain
e-mail: jalfonso@iac.es, jairo@iac.es
[4] Departamento de Astrofísica, Universidad de La Laguna, C/ Astrofísico Francisco Sánchez, 38205 La Laguna, Spain

ABSTRACT

Context. The tumbling pattern of a bar is the main parameter characterising its dynamics. From numerical simulations, its evolution since bar formation is tightly linked to the dark halo in which the bar is formed through dynamical friction and angular momentum exchange. Observational measurements of the bar pattern speed with redshift can restrict models of galaxy formation and bar evolution.
Aims. We aim to determine, for the first time, the bar pattern speed evolution with redshift based on morphological measurements.
Methods. We have selected a sample of 44 low inclination ringed galaxies from the SDSS and COSMOS surveys covering the redshift range $0< z <0.8$ to investigate the evolution of the bar pattern speed. We have derived morphological ratios between the deprojected outer ring radius (R_{ring}) and the bar size (R_{bar}). This quantity is related to the parameter $\mathcal{R} = R_{\rm CR}/R_{bar}$ used for classifiying bars in slow and fast rotators, and allow us to investigate possible differences with redshift.
Results. We obtain a similar distribution of R at all redshifts. We do not find any systematic effect that could be forcing this result.
Conclusions. The results obtained here are compatible with both, the bulk of the bar population ($\sim$ 70%) being fast-rotators and no evolution of the pattern speed with redshift. We argue that if bars are long-lasting structures, the results presented here imply that there has not been a substantial angular momentum exchange between the bar and halo, as predicted by numerical simulations. In consequence, this might imply that the discs of these high surface-brightness galaxies are maximal.

Key words. Galaxies: high-redshift – Galaxies: evolution– Galaxies: structure– Galaxies: kinematics and dynamics

1. Introduction

Stellar bars are thought to be the main internal mechanism driving the dynamical and secular evolution of disc galaxies. They are able to modify the central structure and morphology of galaxies, mostly because they are responsible for a substantial redistribution of mass and angular momentum in the discs (e.g., Sellwood, 1981; Sellwood & Wilkinson, 1993; Pfenniger & Friedli, 1991; Athanassoula, 2003; Debattista et al., 2006). In the last decade, numerical simulations have addressed the importance of the transference of angular momentum between baryonic and dark matter components (e.g., Debattista & Sellwood, 1998, 2000). The amount of angular momentum exchanged is related to the specific properties of the galaxies, such as the bar mass, halo density, and halo velocity dispersion (Debattista & Sellwood, 1998; Athanassoula, 2003; Sellwood & Debattista, 2006) and it takes place mainly at the disc resonances (Athanassoula, 2003; Martinez-Valpuesta et al., 2006). Recent works have shown that gas fraction can also play an important role in the bar-halo interplay and therefore in the bar evolution (Bournaud & Combes, 2002; Romano-Díaz et al., 2009; Villa-Vargas et al., 2010). Moreover, bars are efficient at funneling material toward the galaxy centre and possibly they influence the building of the stellar bulge (e.g., Kormendy & Kennicutt, 2004) and the central black hole (e.g., Shlosman et al., 1989; Regan & Mulchaey, 1999; Corsini et al., 2003). Peanut/boxy bulges in galaxies are also thought to be associated with bending instabilities and bar vertical resonances (Bureau & Freeman, 1999; Debattista et al., 2004, 2006; Athanassoula, 2005; Martinez-Valpuesta et al., 2006; Méndez-Abreu et al., 2008).

As already mentioned, the bar formation and destruction rate, as well as the morphological and dynamical changes suffered by the discs during their lifetime are strongly affected by the angular momentum exchange. Therefore, the cosmological evolution of the bar fraction can also depend on this effect. Observations show that bars in low redshift galaxies are ubiquitous, with a fraction of ∼45% at visual wavelengths (e.g., Marinova & Jogee, 2007; Reese et al., 2007; Barazza et al., 2008; Aguerri et al., 2009; Masters et al., 2011) and rising to ∼70% in the near-infrared (Knapen et al., 2000; Eskridge et al., 2000; Menéndez-Delmestre et al., 2007). The bar fraction depends on morphological type, being lower in lenticular galaxies than in spirals (Marinova & Jogee 2007; Aguerri et al. 2009; Nair & Abraham 2010; Barway et al. 2011; but see also Masters et al. 2011). Some recent results show that bar fraction is a strong function of galaxy mass (Méndez-Abreu et al., 2010; Nair & Abraham, 2010) and color (Hoyle et al., 2011). In contrast, bar fraction is only barely affected by the environment (Aguerri et al., 2009; Li et al., 2009; Méndez-Abreu et al., 2010).

The evolution of the bar fraction with redshift is still a matter of debate. Abraham et al. (1999) found that the fraction of barred galaxies at $z > 0.5$ is lower than the local fraction. However, other authors claim that this may be the consequence of selection effects, due to the high angular resolution needed to find

bars (Elmegreen et al. 2004; but see van den Bergh 2002). To deal with the angular resolution problem, several studies have carried out this analysis using the Advanced Camera for Surveys (ACS) on the Hubble Space Telescope (HST). Thus, Elmegreen et al. (2004) and Jogee et al. (2004) found the same bar fraction (~40%) at redshift $z = 1.1$ as in the local Universe, suggesting that the bar dissolution cannot be common during a Hubble time unless the bar formation rate is comparable to the bar destruction rate. On the contrary, Sheth et al. (2008), in a recent study using images from the Cosmological Evolution Survey (COSMOS; Scoville et al., 2007) and using a larger sample than previous studies, found that the bar fraction at $z = 0.84$ is one-third of the present-day value. They also found a much stronger evolution for low mass galaxies and late-type morphological types. Part of the differences may be due to the selection effects and other systematic effects that still need to be investigated further.

In any case, these results show that bars have been common structural components of the discs of galaxies during the last 8 Gyrs. The study of their origin and evolution could be crucial for understanding the galaxy evolution since $z = 1$. This study can be done by analysing three parameters that characterise the bars: length, strength and pattern speed. Several methods and techniques have been proposed in order to measure these bar parameters. The bar length has been obtained directly by visual inspection on galaxy images (Kormendy, 1979; Martin, 1995; Méndez-Abreu et al., 2010; Nair & Abraham, 2010; Masters et al., 2011), searching for the maximum ellipticity of the galaxy isophotes (Wozniak et al., 1995; Laine et al., 2002; Marinova & Jogee, 2007; Aguerri et al., 2009), locating variations of the isophotal position angle (Sheth et al., 2003; Erwin, 2005), analyzing Fourier moments (Quillen et al., 1994; Aguerri et al., 2000a, 2003), or by photometric decomposition of the surface-brightness profiles of galaxies (Prieto et al., 1997, 2001; Aguerri et al., 2005; Laurikainen et al., 2005; Gadotti, 2008; Weinzirl et al., 2009; Gadotti, 2011). The resulting studies reported that the typical bar length is about 3-4 kpc, and strongly correlates with the disc scale-length (Aguerri et al., 2005; Pérez et al., 2005; Erwin, 2005; Marinova & Jogee, 2007; Laurikainen et al., 2007). Bar length is also a function of galaxy size, morphology and color (Aguerri et al., 2009; Hoyle et al., 2011).

The bar strength has been determined by measuring bar torques (Buta & Block, 2001), isophotal ellipticity (Martinet & Friedli, 1997; Aguerri, 1999; Whyte et al., 2002; Marinova & Jogee, 2007), or Fourier modes (Ohta et al., 1990; Aguerri et al., 2000a; Laurikainen et al., 2005; Athanassoula & Misiriotis, 2002). This parameter depends on galaxy morphology. Bars in lenticular galaxies are generally weaker than in spirals (Das et al. 2003; Laurikainen et al. 2007; Barazza et al. 2008; Aguerri et a. 2009; Buta et al. 2010).

The bar pattern speed, Ω_b, is the main kinematic observable and describes the dynamics of the bar. This tumbling pattern determines the position of the resonances in the disc and it is most usefully parametrised by a distance independent parameter $\mathcal{R} = R_{CR}/R_{bar}$, where R_{CR} is the Lagrangian/corotation radius, where the gravitational and centrifugal forces cancel out in the rest frame of the bar, and R_{bar} is the bar semi-major axis. Therefore, bars that end near corotation ($1< \mathcal{R} <1.4$) are considered fast, while shorter bars ($\mathcal{R} >1.4$) are commonly called slow. If $\mathcal{R} < 1.0$ then orbits are elongated perpendicular to the bar, and self consistent bars cannot exist in this regime (Contopoulos, 1980). The most reliable method for obtaining the location of corotation was that proposed by Tremaine & Weinberg (1984, hereafter TW method) which uses a set of simple kinematic measurements to derive the bar pattern speed assuming that the tracer obeys the continuity equation, that the discs are flat and that there is one well defined pattern speed. However, large integration times are required in medium-size telescopes to reach the high signal-to-noise required to apply the TW method. This limits its application to a small number of candidates. Despite the difficulties in obtaining bar pattern speeds, a reasonable number of nearby galaxies have been investigated (Merrifield & Kuijken, 1995; Debattista et al., 2002; Aguerri et al., 2003; Corsini et al., 2007) finding that all bars end near corotation. Some of these assumptions are not applicable for galaxies with nested bars, and there is now a simple extension of the TW method to multiple pattern speeds (Maciejewski, 2006; Corsini et al., 2003; Meidt et al., 2009) and the fact that some authors have shown that the TW method can be applied to CO (Rand & Wallin, 2004; Zimmer et al., 2004) and H_α velocity fields (Hernandez et al., 2005; Emsellem et al., 2006; Fathi et al., 2007; Chemin & Hernandez, 2009; Gabbasov et al., 2009; Fathi et al., 2009) opens a new window to these studies.

Some indirect ways to derive the bar pattern speed include methods based on numerical modelling: generating either self-consistent models or models using potentials derived from the light distributions (Duval & Athanassoula, 1983; Lindblad et al., 1996; Laine et al., 1998; Weiner et al., 2001; Pérez et al., 2004; Zánmar Sánchez et al., 2008) and then matching numerical experiments with the observed velocity fields; or by matching numerical simulations to the galaxy morphology (Hunter et al., 1988; England, 1989; Laine et al., 1998; Aguerri et al., 2001; Rautiainen et al., 2005). Other indirect methods to derive the bar pattern speed include identifying morphological or kinematic features with resonances: using a variety of features (Elmegreen & Elmegreen, 1990); the shape of dust lanes (Athanassoula, 1992); the sign inversion of the radial streaming motion across corotation (Canzian, 1993); rings as resonance indicators (Buta, 1986; Buta et al., 1995); phase-shift between the potential and density wave patterns (Zhang & Buta, 2007); location of minimum of star formation (Cepa & Beckman, 1990; Aguerri et al., 2000a); or comparison of the behaviour of the phase Fourier angle in blue and near-infrared images (Puerari & Dottori, 1997; Aguerri et al., 1998). Although possibly the most accurate indirect method to calculate pattern speeds is the the comparison of gas velocities to those obtained in numerical simulations that use a potential obtained from optical or near-infrared light, it is also very time consuming and can only be applied to a relatively small number of objects.

The technique to determine the bar pattern speed based on connecting the location of rings to orbital resonances was introduced by Buta (1986). It is based on the theoretical work presented by Schwarz in a series of papers (Schwarz, 1981, 1984b,a) showing how these ring structures appear near the dynamical Lindblad resonances due to a bar–like perturbation. To directly apply this method to find the specific value of the pattern speed not only the location of the ring and the association to a resonance is required, but some kinematic information is also needed. However, we can use the $\mathcal{R}$ parametrisation of the bar introduced previously, and determine the ratio between the outer ring radius (linked to the outer Lindblad resonance, OLR) and the bar length. In this way, we can indirectly determine, not the pattern speed, but whether the bars measured are in the slow or fast regime.

The bar parameters discussed above have been analysed in local galaxy samples. There are no previous studies in the literature about the evolution of the length, strength and pattern speed of bars. In this article, we study for the first time, the dy-

namical evolution of bars with redshift, going from the local Universe to $z \sim 0.8$. We use a well selected sample of barred galaxies with outer rings to exploit the power of this method. The study of the dynamical evolution of bars is critical to constrain the angular momentum exchange between the disc and the halo and their subsequent evolution. Weinberg (1985) predicted that a bar would lose angular momentum due to a massive dark matter halo through dynamical friction, slowing down in the process. This prediction was further confirmed in numerical simulations (Debattista & Sellwood, 1998, 2000; Athanassoula, 2003; Sellwood & Debattista, 2006) where they found that bars are slowed efficiently if a substantial density of dark matter is present in the region of the bar. On the other hand, if the mass distribution is dominated by the stellar disc, then the bar remains rapidly rotating for a long time. We show in this work that bars do not show a systematic change in their dynamical state in the last ~ 7 Gyrs.

The article is organised as follows: we present the sample selection and morphology discussion in Sect. 2. We describe the method followed to measure the ring and bar radius in Sect. 3. The results are presented in Sect. 4 and we discuss their implications in Sect. 5. Conclusions are provided in Sect. 6. Throughout the paper the cosmological parameters used are: $H_0 = 70$ km s^{-1} Mpc^{-1}, $\Omega_\Lambda = 0.7$, and $\Omega_m = 0.3$.

2. Sample selection

The galaxy samples studied in this article were extracted from two different surveys: low redshift galaxies were taken from the Sloan Digital Sky Survey (SDSS; $0.01 < z < 0.04$), and high redshift galaxies were selected from COSMOS ($0.125 < z < 0.75$).

Two caveats must be discussed before the samples are described in detail: first, it is worth noticing that the galaxy samples are not meant to be complete in any sense, however, the selection criteria make the two samples fully comparable. Second, in Aguerri et al. (2009) we studied how the resolution of the SDSS images can affect our detection of bars. We worked out, using artificial galaxies, that the shortest bars that we are able to resolve have a length of ~ 9 pixels. Considering a mean PSF in our SDSS images with a FWHM of 1.″09 (2.77 pixel), we conclude that we resolve bars larger than $\sim 3\times$ FWHM, or equivalently, ~ 0.5 kpc at $z = 0.01$ and ~ 2 kpc at $z = 0.04$. The COSMOS sample was selected using the ACS data in the F814W filter. The images were processed to a resolution of 0.″05 pixel^{-1} with an averaged PSF FWHM of 0.″097 (Scoville et al., 2007; Koekemoer et al., 2007). Based on the previous considerations, we will resolve bars larger than $\sim 3\times$FWHM which corresponds to ~ 0.6 kpc at $z = 0.125$ and ~ 2.2 kpc at $z = 0.75$, matching perfectly the SDSS spatial resolution in the low redshift range.

2.1. Outer Ring Morphological Classification

The ring morphological classification used in this study is based on the work of Buta & Crocker (1991). They divide the outer rings in three main morphological classes resembling the rings developed in numerical simulations near the OLR (Schwarz, 1981). The first class, called R'_1, is characterised by a 180° winding of the spiral arms with respect to the ends of a bar. The second type is known as an R'_2 ring. It is defined by a 270° winding of the outer arms with respect to the bar ends, so that in two opposing quadrants the arm pattern is doubled. The R'_1 and R'_2 morphologies were predicted by Schwarz (1981) as the kind of patterns that would be expected near the OLR in a barred galaxy. The third class is referred to in Buta & Crocker (1991) as the $R_1R'_2$ morphology, where the outer arms break not from the ends of the bar, but from an R'_1-type ring. The existence of this combined type, which may be linked to the population of both main families of OLR periodic orbits (Schwarz, 1981), provides some of the clearest evidence of the OLR in barred galaxy morphology. Some examples of this classification, taken from our sample of low and high redshift galaxies, are shown in Fig. 1. Buta et al. (1995) derived the distribution of intrinsic axis ratios for the outer rings using the Catalog of Southern Ringed Galaxies. They found that outer rings present in barred galaxies are intrinsically elliptical with an axis ratio $\sim 0.82 \pm 0.07$, and that the intrinsic ellipticity varies from the R'_1 ($\sim 0.74 \pm 0.08$) to the R'_2 ($\sim 0.87 \pm 0.08$). The intrinsic shape of the rings plays an important role when deprojecting distances such as the bar length and the ring radius, thus, more intrinsically elliptical rings will increase the uncertainties in the measurements. We decided to remove from our samples the R'_1 type of rings, and keep only the R'_2 types since they are intrinsically rounder. In fact, their intrinsic shape is very similar to that of typical discs (Fasano et al., 1993; Ryden, 2004).

2.2. Low redshift

The barred ringed galaxies at low redshift were obtained from the galaxy sample analysed in Aguerri et al. (2009). They selected a volume limited sample of galaxies from the spectroscopic catalogue of the SDSS Data Release 5 (SDSS-DR5, Adelman-McCarthy et al. 2007). This sample covers the redshift range $0.01 < z < 0.04$, down to an absolute magnitude of $M_r < -20$, and with low inclination $i < 60°$. The full sample consist of 3060 galaxies with a morphological mix of 26% ellipticals, 29% lenticulars, 20% early type spirals, and 25% late type spirals. Galaxies were classified in barred and unbarred systems by searching for absolute maxima in the ellipticity radial profiles of their isophotes (see Aguerri et al. 2009 for details). From the barred sample we visually inspected the SDSS galaxy images in order to look for the presence of outer rings of type R'_2.

We obtained a total of 18 barred galaxies with suitable outer rings features. Table 1 shows the main properties of the bars and rings features measured in these galaxies.

2.3. High redshift

As for the low redshift sample, we have chosen a number of low inclination galaxies from the third release of the COSMOS HST survey (Scoville et al., 2007). We first downloaded all the 81 image tiles from the COSMOS/ACS fields, observed using the F814W (I-band) filter, from the Multimission Archive at STScI (MAST[1]) for visual inspection. These observations cover ~ 2 deg^2 with a pixel scale (for the drizzled data) of 0.″05 pixel^{-1}.

We visually scanned the COSMOS fields to look for clearly ringed barred galaxies. After a preliminary list was created, we correlated the positions with the spectroscopic redshifts from the Very Large Telescope (VLT) and Magellan COSMOS spectroscopic surveys (zCOSMOS Survey; Lilly et al. 2007) to search for candidates with reliable redshifts. We searched also for photometric redshifts for the remaining candidates. We used photometric redshifts determined by Faure et al. (2008) using the

[1] Based on observations made with the NASA/ESA Hubble Space Telescope, obtained from the data archive at the Space Telescope Science Institute. STScI is operated by the Association of Universities for Research in Astronomy, Inc. under NASA contract NAS 5-26555.

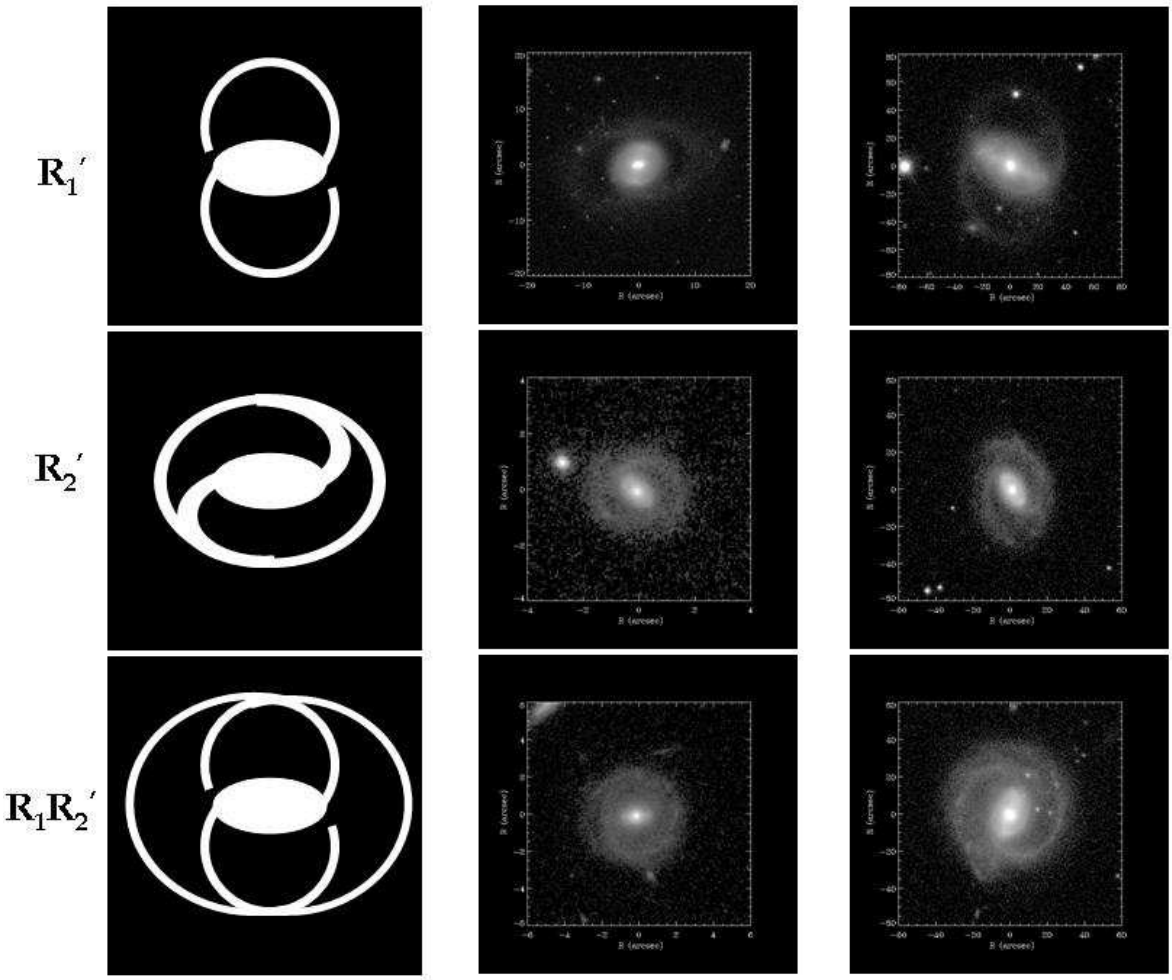

Fig. 1: Left column: schematic view of the different ring types in barred galaxies (see Sect. 2.1). Ring type examples of barred galaxies at high (middle column), and low (right column) redshifts.

Le Phare photometric redshift estimation code (Ilbert et al. 2006), details concerning the multi-wavelength photometry can be found in Mobasher et al. (2007). Faure et al. (2008) used 1095 spectroscopic redshifts from the zCOSMOS Survey (Lilly et al. 2006) to calibrate the ground-based photometric zero points. Using eight bands, this method achieves a photometric redshift accuracy of $\sigma_{\Delta z}/(1+z_s)$=0.031.

From this sample, only galaxies showing type R_2' ring were included in the sample. Finally the high redshift sample consists of 26 galaxies. The main properties of the bars and rings features are shown in Table 2. The sample covers the redshift range $0.125 < z < 0.75$. Figure 2 shows the redshift distribution.

3. Outer ring radius and bar size definition

Our approach to quantifying the dynamical state of the bars in our sample of ringed galaxies is based on the measurements of both the bar and ring radius. We deproject bar size in the plane of the galaxy using i, the galaxy inclination, and θ, the position angle of the galaxy component (bar or ring). We assume that the outer ring reflects the properties of the disc, and therefore that the ellipticity and position angle of the ring and disc are the same. In Sect. 2.1 we have discussed that both components are intrinsically similar and possible differences will only affect our results by introducing a large scatter. Under this hypothesis, the ring radius does not need to be deprojected, since it is measured along the major axis of the galaxy, and the galaxy inclination can be derived simply by $i = \arccos(1 - \epsilon_{\rm ring})$.

3.1. Ellipse fitting

The low redshift sample measurements were derived by using the ellipticity and position angle radial profiles extracted from the symmetrised images. This approach allows us to clean the images from spurious sources. It works as follows: each image is rotated 180° with respect to the galaxy centre. Then, we subtract the rotated frame from the original one. The residual image was sigma-clipped to identify all the pixels with a number of counts lower than 1σ, where σ is the r.m.s. of the image background. The value of the deviant pixels was set to zero. Finally, the cleaned image was subtracted from the original one to get the symmetrised image. The ellipses were then fitted to the isophotes

Table 1: General properties of the SDSS sample.

Name	$R_{bar-min}$ (kpc)	$R_{bar-max}$ (kpc)	PA_{bar} (degrees)	ϵ_{ring}	PA_{ring} (degrees)	R_{ring} (kpc)	z
(1)	(2)	(3)	(4)	(5)	(6)	(7)	(8)
SDSSJ104924.86-002547.5	6.6	5.1	121.6±0.9	0.402±0.004	142.2±0.8	13.0	0.039
SDSSJ102543.29+393846.9	7.3	5.1	153.4±0.2	0.075±0.005	74.8±2.3	13.0	0.023
SDSSJ122529.23+471623.4	5.7	4.7	11.6±0.1	0.174±0.005	30.1±14.3	10.8	0.025
SDSSJ130235.73+411924.1	4.8	3.7	165.4±0.7	0.186±0.005	45.4±1.5	9.9	0.028
SDSSJ120732.62+324846.7	7.1	4.7	54.4±0.5	0.084±0.007	74.1±20.0	11.6	0.026
SDSSJ133259.13+321913.6	5.7	3.8	177.3±0.3	0.044±0.007	106.7±8.6	8.7	0.035
SDSSJ012858.63-005656.3	8.0	6.3	6.2±0.3	0.341±0.002	83.6±0.4	16.4	0.018
SDSSJ083220.43+412132.0	3.5	2.4	52.8±0.5	0.048±0.005	111.3±10.9	7.9	0.025
SDSSJ083630.84+040215.6	6.6	4.5	94.2±0.2	0.164±0.009	37.0±3.8	12.7	0.029
SDSSJ091426.23+360644.1	6.3	5.0	164.4±0.0	0.163±0.031	156.1±1.0	10.1	0.022
SDSSJ123234.57+492312.2	5.3	3.4	176.1±0.5	0.074±0.012	114.1±10.7	8.7	0.040
SDSSJ142412.12+350846.0	3.6	2.7	45.3±1.0	0.238±0.006	52.9±26.7	9.3	0.029
SDSSJ153619.30+493428.3	5.3	2.9	17.8±2.1	0.211±0.006	73.1±0.7	9.7	0.038
SDSSJ160331.62+492017.3	8.7	5.2	70.9±0.4	0.255±0.005	32.3±7.2	16.9	0.020
SDSSJ172721.89+593837.6	5.9	4.0	171.3±0.1	0.202±0.004	148.8±1.1	11.4	0.028
SDSSJ123313.69+121449.2	3.9	3.1	118.5±0.9	0.023±0.004	65.3±11.5	6.9	0.026
SDSSJ120609.11-025653.2	5.3	3.9	61.5±0.7	0.149±0.009	17.3±4.6	11.2	0.026
SDSSJ111044.88+043039.0	6.8	5.0	97.6±0.2	0.062±0.007	64.6±9.2	12.5	0.029

NOTE. Col. (1): Galaxy name from SDSS; Col. (2): bar radius calculated using the position of the minimum ellipticity; Col. (3): bar radius calculated using the position of the maximum ellipticity; Col. (4): position angle of the bar; Col. (5): ring ellipticity; Col. (6): position angle of the ring; Col. (7): ring radius; Col. (8): spectroscopic redshift from SDSS

Table 2: General properties of the COSMOS sample

Name	$R_{bar-min}$ (kpc)	$R_{bar-max}$ (kpc)	PA_{bar} (degrees)	ϵ_{ring}	PA_{ring} (degrees)	R_{ring} (kpc)	z
(1)	(2)	(3)	(4)	(5)	(6)	(7)	(8)
812947	5.4	4.1	76.3±0.1	0.068±0.010	120.5±14.8	9.8	0.125 (*s*)
816960	5.5	3.4	174.8±1.2	0.059±0.035	85.2±22.6	7.5	0.311 (*s*)
J095928.30+020109.0	5.3	3.8	63.2±0.6	0.088±0.045	141.3±41.8	9.1	0.530 (*p*)
817887	5.6	4.6	116.2±2.8	0.056±0.028	88.4±17.5	15.1	0.672 (*s*)
823705	3.6	2.7	46.4±0.7	0.165±0.028	74.4±17.2	6.3	0.491 (*s*)
824759	3.7	2.9	136.1±1.8	0.161±0.023	158.1± 7.0	7.0	0.751 (*s*)
825492	5.1	3.6	108.4±2.4	0.152±0.057	108.1±22.2	8.7	0.736 (*s*)
833039	4.3	3.3	100.6±1.1	0.203±0.056	32.8± 4.8	8.8	0.360 (*s*)
J100233.98+022524.3	4.7	2.2	172.7±0.9	0.167±0.015	63.1± 4.4	9.4	0.720 (*p*)
J095938.81+020658.7	10.3	7.6	111.7±0.4	0.071±0.035	149.6±75.9	16.6	0.409 (*p*)
J095935.08+020127.2	4.3	3.0	176.8±79.2	0.158±0.044	26.3±36.9	10.3	0.357 (*p*)
J100204.95+022739.7	5.8	3.7	124.4±1.0	0.116±0.019	122.7± 6.6	10.5	0.507 (*p*)
841055	5.7	3.4	134.9±0.6	0.188±0.020	178.0±56.2	13.7	0.376 (*s*)
J095759.45+022810.5	4.4	2.6	20.6±0.9	0.042±0.013	131.0±23.0	9.2	0.119 (*s*)
851598	6.4	4.4	9.6±0.5	0.080±0.047	102.2±30.7	10.0	0.346 (*s*)
852495	6.8	5.7	96.7 ±3.1	0.265±0.015	21.9± 1.5	12.2	0.705 (*s*)
852636	7.1	4.9	0.7±80.0	0.040±0.026	125.6±50.7	12.5	0.345 (*s*)
852155	7.7	5.6	173.0±0.3	0.306±0.009	160.4± 0.8	15.3	0.305 (*s*)
J100254.88+024645.8	4.4	3.2	18.7±1.5	0.065±0.036	128.0±45.7	8.5	0.468 (*p*)
840577	5.1	3.5	68.3±2.4	0.085±0.023	89.5±15.0	7.9	0.539 (*s*)
838743	4.4	2.8	48.7±0.5	0.144±0.025	60.0±3.8	8.9	0.126 (*s*)
830974	9.6	5.3	11.5±1.4	0.149±0.025	57.7±7.0	13.9	0.695 (*s*)
811921	4.9	3.1	25.2±1.6	0.068±0.027	89.5±30.7	8.2	0.371 (*s*)
813153	7.5	6.0	60.0±0.7	0.159±0.069	47.3±28.1	13.2	0.529 (*s*)
831775	3.6	1.8	125.1±0.1	0.140±0.028	156.8±76.5	6.2	0.381 (*s*)
J100217.12+023024.1	4.9	3.4	157.8±0.8	0.083±0.022	97.7±15.6	8.1	0.379 (*p*)

NOTE. Col. (1): Galaxy name from COSMOS; Col. (2): bar radius calculated using the position of the minimum ellipticity; Col. (3): bar radius calculated using the position of the maximum ellipticity; Col. (4): position angle of the bar; Col. (5): ring ellipticity; Col. (6): position angle of the ring; Col. (7): ring radius; Col. (8): (*s*): spectroscopic redshift from zCOSMOS; (*p*): photometric redshift from Faure et al. (2008).

of the symmetrised images of the galaxies using the IRAF[2] task `ELLIPSE` (Jedrzejewski, 1987). We used an iterative wrapped procedure which runs the ellipse fitting several times, changing

[2] IRAF is distributed by NOAO, which is operated by AURA Inc., under contract with the National Science Foundation.

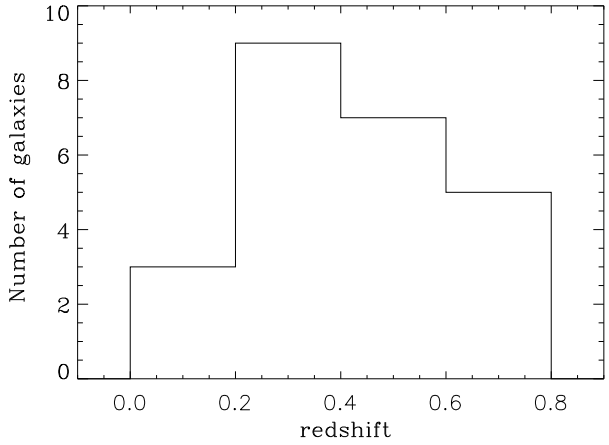

Fig. 2: Redshift distribution for the high redshift sample.

the trial values at each fit iteration, until a good fit at all radii is obtained. At each fixed semi-major axis length, the coordinates of the centre of the fitting ellipse were kept fixed. This centre was identified with the position of the central intensity peak. The trial values for the ellipticity and position angle were randomly chosen between 0 and 1 and between -90° and 90°, respectively. The fitting procedure stopped when either convergence was reached or after 100 iterations.

The high redshift sample ellipticity and position angle profiles were derived using the same wrapping procedure to maximise the goodness of the ellipse fitting. However, in this case we preferred not to symmetrise the images but apply a 2×2 pixels box smoothing. The image symmetrisation was not needed since the sample galaxies were not contaminated by other sources within their projected surface and the smoothing provided better radial profiles by improving the signal-to-noise ratio of the images.

3.2. Bar length

The ellipticity radial profile of a typical barred galaxy reaches a minimum at the centre, because of either seeing effects or a spherical bulge. Then, it usually shows a global increase to a local maximum, and then suddenly decreases towards a minimum at the location where the isophotes become axisymmetric in the face-on case. The position angle profile is also characteristic in barred galaxies, being constant in the bar region and then changing to fit the outer disc orientation (e.g., Wozniak et al., 1995; Aguerri et al., 2000b). These characteristic profiles are produced by the shape and orientation of the stellar orbits of the bar (see Contopoulos & Grosbol, 1989; Athanassoula, 1992). Different methods have been used to measure the bar length based on the ellipticity and position angle radial profiles (see Athanassoula, 2002; Michel-Dansac & Wozniak, 2006). However, the solution is always ambiguous and it can lead to misleading results. In order to remove these uncertainties we decided to measure the bar length as the midpoint between the radius of the maximum and minimum ellipticity. These two different measurements of the bar length represent the extreme cases (Michel-Dansac & Wozniak, 2006) and therefore they represent an upper limit of our errors in the bar radius measurements. We preferred this solution not to bias our conclusions. The position angle of the bar, which is needed to deproject the bar length, was measured at the position of the maximum ellipticity, so we avoid problems related to position angle variation in the bar-disc region. An example of this method applied to three of our low and high redshift galaxies is shown in Figs. 3, 4, respectively.

3.3. Ring radius

As for the bar component, the ring radius was derived based on the ellipticity and position angle radial profiles. In the ring region, we expect that the ellipticity and position angle radial profiles will remain constant due to the stellar orbits in the ring. Therefore, we identify the region of the profile where the ring is present and we measured the ring radius as the position where the ellipticity and position angle become constants. The ring ellipticity and position angle also needed for deprojecting, were derived as a mean of these constant values. The error in the ring radius has been calculated by comparing the estimated ring radius with the radius at which the ellipticity varies more than 3 times the standard deviation of the disc ellipticity. Figures A.1 and A.2 from the Appendix show all the galaxies with the ring radius overplotted.

4. Results

Table 1 and Table 2 shows the obtained parameters for the ring radius, ellipticity, position angle and the bar semi-major axis, as derived in Sect. 3.1. Most galaxy inclinations lie below $i < 40^\circ$. The bar size range, using the maximum ellipticity, covers from 2.5 to 6.3 kpc. Most of the bars in the local Universe (about 70%, see Aguerri et al. 2009) are within this bar size range. Similar values of the bar size range are found for our high redshift galaxies. The mean bar radius of our low and high redshift galaxies are 4.5±1.04 and 3.5±1.33 kpc, respectively. This means that within the errors both galaxy samples have similar bars according to their lengths and similar to local samples of barred galaxies (see Aguerri et al. 2009). The average bar size, using the minimum ellipticity, for our low and high redshift galaxies are also similar: 5.9±1.43 and 5.3±1.70 kpc, respectively. Thus, both samples of galaxies show similar bar sizes independent of the method used for determining the bar length. It has been argued (Michel-Dansac & Wozniak, 2006) that the sizes calculated using the minimum of the ellipticity correlate well with the position of corotation, giving a more physically significant size than measurements obtained with the maximum of the ellipticity, which clearly underestimates the true bar size. To avoid problems related to the bar size calculation, as explained in Sect. 3.2, we have opted for using the mid-point and to take into account the values of R_{bar} using both methods to obtain the errors.

We have determined the strength of the bars for the low and high redshift galaxies by using the maximum ellipticity of the bar (see Aguerri et al. 2009). Both samples cover the same range of bar strengths. Thus, the mean values of the bar strength of our low and high redshift samples are: 0.20±0.07, and 0.17±0.05. These values are similar to the mean strength of bars in the local Universe (0.20±0.07; see Aguerri et al. 2009). We can conclude that according to the size and strength of the bars, our low and high redshift galaxy samples have similar bars as those found in a complete local sample of barred galaxies (see Aguerri et al. 2009).

To determine whether our galaxies are in the *fast* or *slow* range (see Sect.1) we define the ratio $\mathcal{R}_{ring} = R_{ring}/R_{bar}$, where R_{ring} is the ring radius and R_{bar}, is the bar semi-major axis, as

characterised in Sect. 3. Because we cover this ratio for galaxies with redshifts between $0 < z < 0.8$, we can study possible changes of this ratio with redshift. Figure 5 shows the distribution of ring radii (R_{ring}) vs. the bar semi-major axis (R_{bar}) for the whole sample. We consider a fast bar those bars for which the R_{CR}/R_{bar} ratio lies between 1.0 and 1.4. This ratio has been plotted in Fig. 5 for both values and is calculated using linear resonance theory and a flat rotation curve (Athanassoula et al. 1982), in this case the position of the OLR (i.e., the ring radius) and the CR are related in the following way:

$$(\frac{R_{\rm ring}}{R_{\rm CR}})^{\delta} = 1 + (1 - \frac{1}{2}\delta)^{1/2} \quad (1)$$

where δ lies between 0.7 and 1.0 for early type discs, see Athanassoula et al. (1982). We take δ=1.0 in Fig. 5 for simplicity but this choice does not alter the results. It is clear from Fig. 5 that all the galaxies, independent of their redshift bin, fall into the fast-bar category.

We have investigated the influence of the inclination of the galaxies on this result. Thus, the average values for $\mathcal{R}_{ring}$ at different inclinations are the following: i) for the low redshift sample and b/a > 0.9, the average $\mathcal{R}_{ring} = 0.51\pm 0.06$, for b/a < 0.9, the average $\mathcal{R}_{ring} = 0.50 \pm 0.08$ ii) for the high-redshift sample; for b/a > 0.9, the average $\mathcal{R}_{ring} = 0.55 \pm 0.09$ and for b/a < 0.9, the average $\mathcal{R}_{ring} = 0.52 \pm 0.12$. All the values, independently of redshift and inclination are comparable; and therefore, we do not see changes of this ratio with redshift.

5. Discussion

5.1. Possible caveats

The tightness of the results shown in Fig. 5 is somewhat unexpected considering the intrinsic uncertainties inherent to the measurements used in this work. For instance, we have assumed that the outer ring are perfectly circular, which is critical for the deprojection of the ring and bar lengths. In Sect. 3 we justified the assumption of roundness for the R'_2 and $R_1R'_2$ ring morphologies. In addition, we have taken into account the limits of intrinsic axis ratios given in Buta et al. (1995) to calculate the errors in the projected sizes, and we have demonstrated in the previous section that our result does not depend on the inclination of the galaxies. Therefore we conclude that projection effects are not biasing our results.

Another possible caveat to our result might be that the choice of ring galaxies biases the sample towards a certain pattern speed domain. However, numerical simulations (Byrd et al., 1994) have shown that resonant outer rings can be present in both fast and slow bars. All types of ring morphologies are found at different pattern speeds. In the same work, all types of ring morphologies also developed for different bar strengths. Athanassoula et al. (2010), who presented a new theory for ring and spiral formation, argues that there is a connection between the bar strength and the morphology of the rings. Nevertheless, R'_2 rings, as are those selected in this work, are located in barred galaxies with similar bar strengths as our galaxies (see Athanassoula et al. 2010). In addition, they show that R'_2 type rings can be formed in galaxies with fast and slow bars.

Although the bar size as measured in different rest-frame band passes could be different, it has been recently shown (Gadotti 2011) that in fact the difference in bar size is negligible and therefore we are not introducing a bias by measuring the bars a high-redshift near the *g*-band rest-frame while the low-redshift bar sizes are measured from the SDSS *r*−band.

Our low and high redshift samples are by no means complete. Therefore, it is customary to investigate whether this fact is affecting the results presented in Fig. 5. Since our low and high redshift barred galaxies are similar in size and strength we could be biasing the resulting pattern speeds toward a particular regime. In other words, the fact that we have not observed evolution in the pattern speed could be just due to the selection of similar fast bars. However, we know from a study of a complete sample of local barred galaxies (Aguerri et al. 2009), that only 30% of the local bars show larger lengths than our ringed barred galaxies. Studies of high redshift bars, 0.4 < z >0.8, (Jogee et al., 2004; Barazza et al., 2009) have shown that the bar size distribution is similar to that of local galaxies and; therefore, as discussed before, similar to the bars size range of the bars presented in this work. Therefore, we do not seem to be looking at any special type of bar by analysing ringed galaxies. As previously mentioned, from numerical models, bars get longer and slower as they age. We can then set a 30% upper limit to the bars that could have suffered a change in their pattern speed in the last 7 Gyr, assuming that nearby long bars are the end-products of the evolution of fast bars. The remaining 70% of bars did not substantially lose angular momentum to the halo, maintaining their pattern speed. This discussion might be related to an implicit morphological bias, since it remains, even for local galaxies, to derive the pattern speed of bars in very late-type gaseous rich spirals which might suffer an intrinsically different evolution (e.g., Bournaud and Combes 2002).

5.2. Comparison with the results from numerical modelling

A recent numerical work (Villa-Vargas et al., 2010) shows that the evolution of the pattern speed and bar-growth of a bar embedded in a live dark matter halo depends strongly on the gas content. In their simulations, a fixed fraction of the total mass was converted to gas mass, and the evolution of the bar parameters is then followed in time. The presence of gas changes the evolution of both the bar growth and the pattern speed evolution, the addition of gas can stop, or even speed-up, the pattern speed of the bar with time. The bar size is anti-correlated with the disc gas fractions. These gas-rich galaxies would be related to early-type galaxies because the gas leads to larger central mass concentration and therefore larger bulges. The results we present in this paper could be in agreement with these gas-rich models. However, the full picture is still unclear since it is observed that longer bars reside in late-type galaxies (e.g., Erwin 2005) which is against the model predictions. Furthermore, we should then explain why all the galaxies should have started with similar gas fractions in their discs.

There is also the possibility that the bars that we see at $z \sim 0.8$ do not survive till the present and therefore, we do not see evolution because the time-scales involved in the formation and destruction are too short. It has been discussed (see Pfenniger & Norman, 1990; Bournaud & Combes, 2002; Bournaud et al., 2005) that gas-rich bars, i.e., late-type spirals, are short lived, with lifetimes of 1-2 Gyr. This short time scale would mimic a lack of evolution of long-lived bars; however, the galaxies in the sample show morphologies typical of early type spirals and there is evidence, from stellar population studies (Pérez et al., 2009; Sánchez-Blázquez et al., 2011), that bars in early type galaxies are long-lived. If this is the case, and most of the ring galaxies we observe present long-lasting bars, it would imply that bars cannot have grown in time and kept being in the fast speed regime without increasing significantly in size.

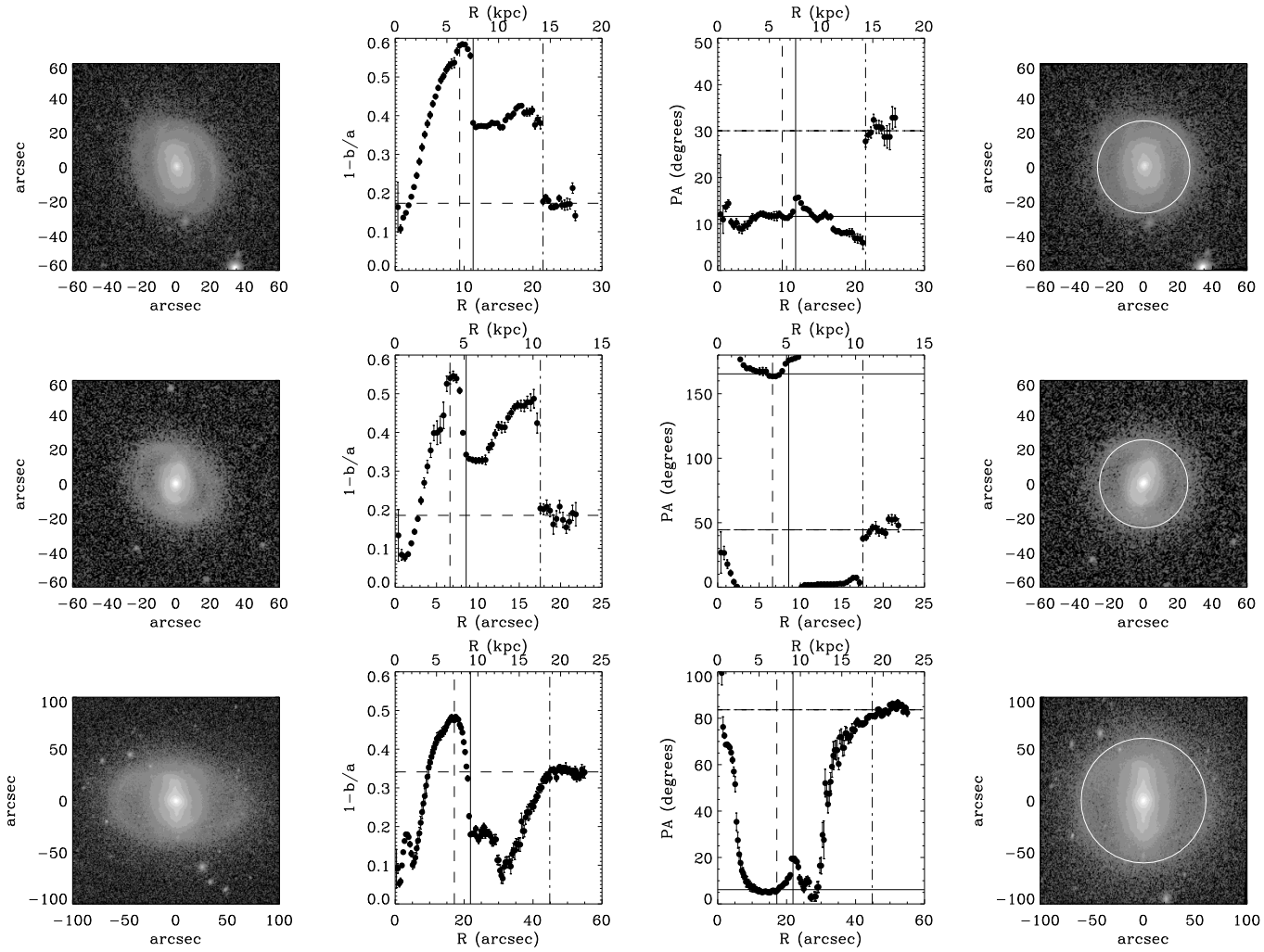

Fig. 3: Three examples of the ringed galaxies selected from the SDSS data. From left to right: original *r*-band SDSS image, ellipticity isophotal radial profile, position angle radial profile of the isophotes, and deprojected image. The vertical full, dashed and dotted-dashed lines represent the $R_{bar-min}$, $R_{bar-max}$, and R_{ring}, respectively. The horizontal full, dashed and dotted-dashed lines shows the PA of the bar, ellipticity of the disc and PA of the disc, respectively. The circle represented in the right-most panels has a radius equal to the measured radius of the ring.

Therefore, the fact that we see the ring radius and the bar size covering the same size range at all redshift, and moreover large bars at high-redshift, implies that bars do not grow significantly in size with time.

The result shown in Fig. 5 implies that bars have not evolved considerably, neither in size nor in pattern speed, since around the time when the Universe was half its present age. Most numerical simulations obtain bars that evolve with time, getting longer and stronger while slowing down (e.g., Debattista &Sellwood 1998; Athanassoula 2003). This effect is mostly due to the angular momentum exchange of the bar-disc system with the dark matter halo. Thus, the fact that bars are compatible with fast rotators at all redshifts indicates that the angular momentum exchange between the bar and halo has not been important enough in the last 7 Gyr to slow down bars. If the pattern speed can be used to set constrains to the halo-to-disc mass ratio, these results might imply that the discs in the high surface-brightness galaxies of our sample are maximal.

6. Summary and conclusions

We have analysed 44 low inclination ringed galaxies spanning a redshift range between $0 < z < 0.8$ to study the possible evolution of the pattern speed in the last 7 Gyrs.

We calculated for each galaxy a morphological parameter indicative of the dynamical state of their bars. In particular, we derived whether they are fast or slow rotators. We find that the bar pattern speed does not seem to change with redshift and that all bars are compatible with being fast bars.

If the bars analysed are long-lasting, their size and bar strength have not significantly changed in time. The fact that, independent of the redshift, the bars are fast rotators and their size has not significantly changed in time could have also large implication for bar evolution models that mostly predict a bar growth with time. It has been argued that the exchange of angular momentum with a centrally dense halo causes the bar to evolve; however the present results might imply that the disc in the high surface-brightness galaxies is maximal and the central mass density is dominated by the stellar component which would lower the angular momentum exchange between the disc

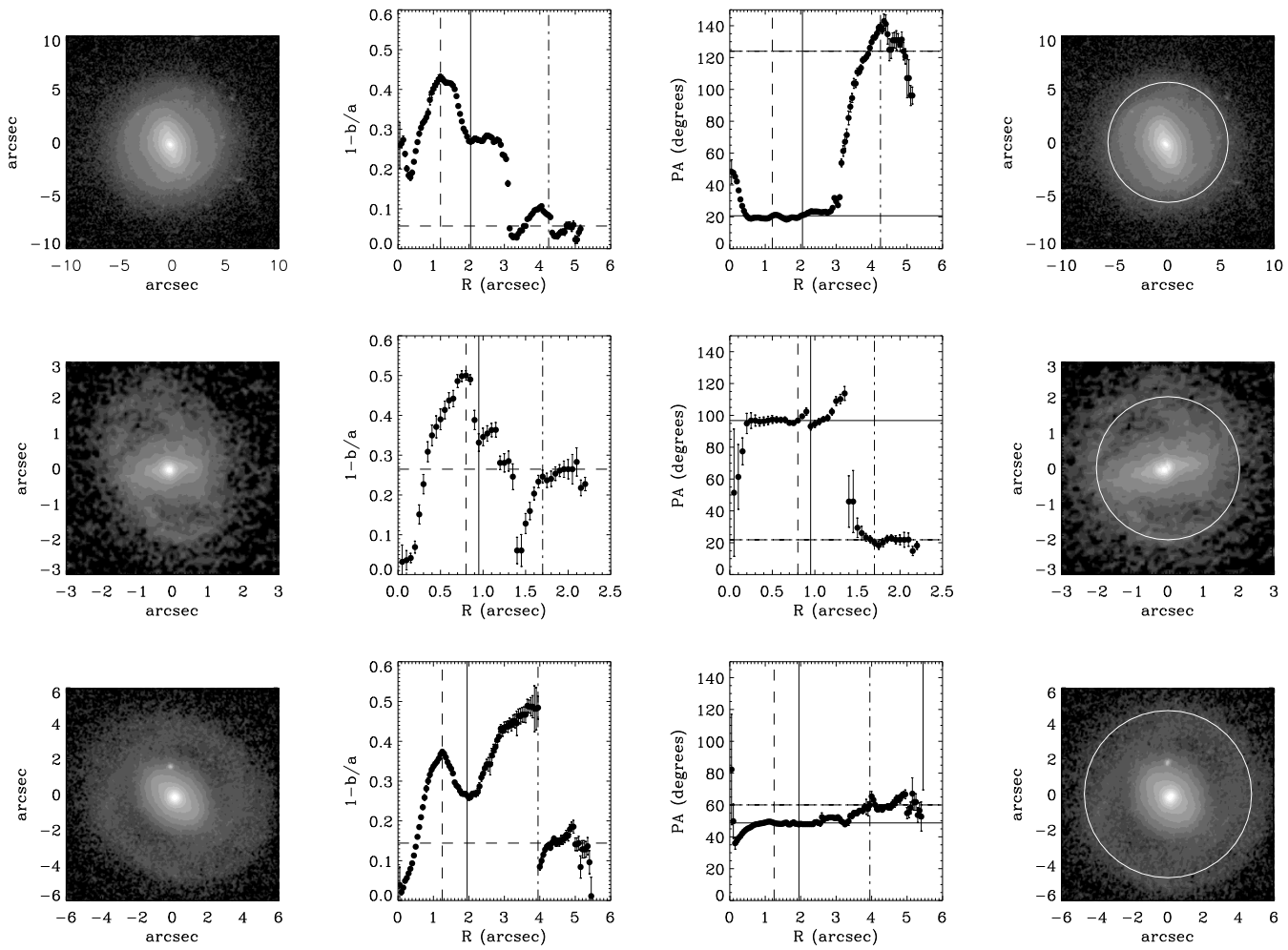

Fig. 4: Three examples of the ringed galaxies selected from the COSMOS data. From left to right: original r-band COSMOS image, ellipticity isophotal radial profile, position angle radial profile of the isophotes, and deprojected image. The vertical full, dashed and dotted-dashed lines represent the $R_{bar-min}$, $R_{bar-max}$, and R_{ring}, respectively. The horizontal full, dashed and dotted-dashed lines shows the PA of the bar, ellipticity of the disc and PA of the disc, respectively. The circle represented in the right-most panels has a radius equal to the measured radius of the ring.

and the halo and slow down the bar evolution (e.g., Debattista & Sellwood, 2000, but for a different conclusion, see Athanassoula, 2003).

This is the first time that the pattern speed evolution has been investigated from the observational point of view. The results presented here place strong constrains on the bar evolution models.

Acknowledgements. We thank the referee for his/her useful comments. We would like to thank Victor Debattista for the careful reading of the manuscript. I.P. was supported by the Spanish Ministry of Science and Innovation (MICINN) (via grants AYA2010-21322-C03-02, AYA2010-21322-C03-03, AYA2007-67625-C02-02 and Consolider-Ingenio CSD2010-00064) and by the Junta de Andalucía (FQM-108). JALA and JMA were supported by the projects AYA2010-21887-C04-04 and by the Consolider-Ingenio 2010 Program grant CSD2006-00070.

References

Abraham, R. G., Merrifield, M. R., Ellis, R. S., Tanvir, N. R., & Brinchmann, J. 1999, MNRAS, 308, 569
Adelman-McCarthy, J. K., Agüeros, M. A., Allam, S. S., et al. 2007, ApJS, 172, 634
Aguerri, J. A. L. 1999, A&A, 351, 43
Aguerri, J. A. L., Beckman, J. E., & Prieto, M. 1998, AJ, 116, 2136
Aguerri, J. A. L., Debattista, V. P., & Corsini, E. M. 2003, MNRAS, 338, 465
Aguerri, J. A. L., Elias-Rosa, N., Corsini, E. M., & Muñoz-Tuñón, C. 2005, A&A, 434, 109
Aguerri, J. A. L., Hunter, J. H., Prieto, M., et al. 2001, A&A, 373, 786
Aguerri, J. A. L., Méndez-Abreu, J., & Corsini, E. M. 2009, A&A, 495, 491
Aguerri, J. A. L., Muñoz-Tuñón, C., Varela, A. M., & Prieto, M. 2000a, A&A, 361, 841
Aguerri, J. A. L., Varela, A. M., Prieto, M., & Muñoz-Tuñón, C. 2000b, AJ, 119, 1638
Athanassoula, E. 1992, MNRAS, 259, 345
Athanassoula, E. 2002, ApJ, 569, L83
Athanassoula, E. 2003, MNRAS, 341, 1179
Athanassoula, E. 2005, MNRAS, 358, 1477
Athanassoula, E., Bosma, A., Creze, M., & Schwarz, M. P. 1982, A&A, 107, 101
Athanassoula, E. & Misiriotis, A. 2002, MNRAS, 330, 35
Athanassoula, E., Romero-Gómez, M., Bosma, A., & Masdemont, J. J. 2010, MNRAS, 407, 1433
Barazza, F. D., Jablonka, P., Desai, V., et al. 2009, A&A, 497, 713
Barazza, F. D., Jogee, S., & Marinova, I. 2008, ApJ, 675, 1194
Barway, S., Wadadekar, Y., & Kembhavi, A. K. 2011, MNRAS, 410, L18
Bournaud, F. & Combes, F. 2002, A&A, 392, 83
Bournaud, F., Combes, F., & Semelin, B. 2005, MNRAS, 364, L18
Bureau, M. & Freeman, K. C. 1999, AJ, 118, 126

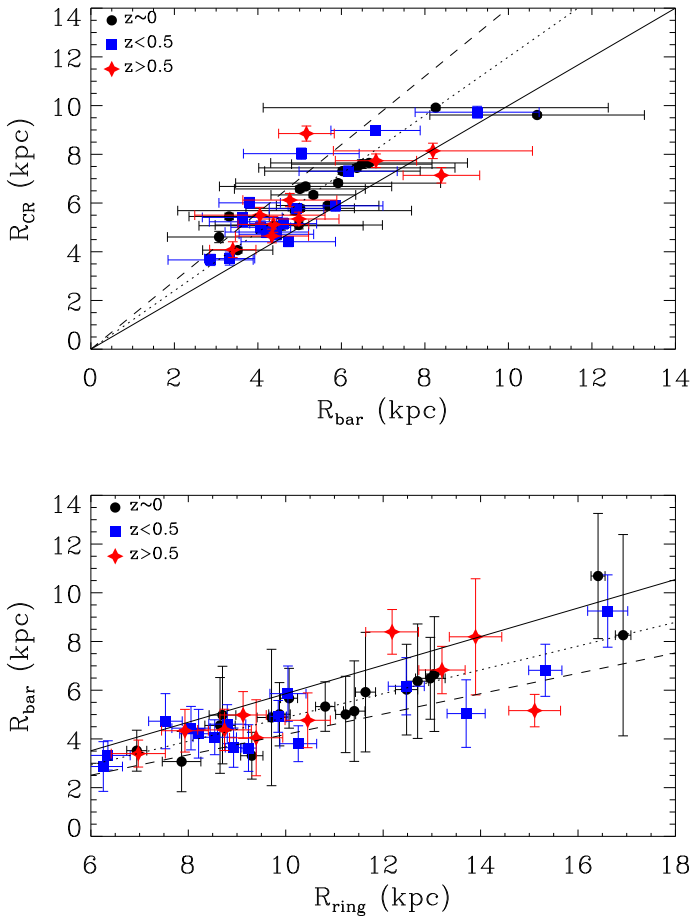

Fig. 5: Top panel: bar semi-major axis vs. corotation radius for both high and low redshift sample. The sample has been divided in three redshift bins; z≈0 (solid black circles), z < 0.5 (solid blue squares), and z > 0.5 (solid red stars). The solid, dotted and dashed lines represent the values, from linear theory, of $\mathcal{R} = R_{\rm CR}/R_{\rm bar} = 1.0, 1.2$ and 1.4, respectively. This range corresponds to what it is considered in the literature as fast bars (see Sect. 1). Bottom panel: outer ring radius vs. bar semi-major axes radius for both high and low redshift sample, the symbols and lines are the same as the ones represented in the top panel. Notice that all galaxies, regardless of their redshift, clearly fall into the 'fast-bar' region. .

Buta, R. 1986, ApJS, 61, 609
Buta, R. & Block, D. L. 2001, ApJ, 550, 243
Buta, R. & Crocker, D. A. 1991, AJ, 102, 1715
Buta, R., Laurikainen, E., Salo, H., & Knapen, J. H. 2010, ApJ, 721, 259
Buta, R., van Driel, W., Braine, J., et al. 1995, ApJ, 450, 593
Byrd, G., Rautiainen, P., Salo, H., Buta, R., & Crocher, D. A. 1994, AJ, 108, 476
Canzian, B. 1993, ApJ, 414, 487
Cepa, J. & Beckman, J. E. 1990, ApJ, 349, 497
Chemin, L. & Hernandez, O. 2009, A&A, 499, L25
Contopoulos, G. 1980, A&A, 81, 198
Contopoulos, G. & Grosbol, P. 1989, A&A Rev., 1, 261
Corsini, E. M., Aguerri, J. A. L., Debattista, V. P., et al. 2007, ApJ, 659, L121
Corsini, E. M., Debattista, V. P., & Aguerri, J. A. L. 2003, ApJ, 599, L29
Das, M., Teuben, P. J., Vogel, S. N., et al. 2003, ApJ, 582, 190
Debattista, V. P., Carollo, C. M., Mayer, L., & Moore, B. 2004, ApJ, 604, L93
Debattista, V. P., Corsini, E. M., & Aguerri, J. A. L. 2002, MNRAS, 332, 65
Debattista, V. P., Mayer, L., Carollo, C. M., et al. 2006, ApJ, 645, 209
Debattista, V. P. & Sellwood, J. A. 1998, ApJ, 493, L5+
Debattista, V. P. & Sellwood, J. A. 2000, ApJ, 543, 704
Duval, M. F. & Athanassoula, E. 1983, A&A, 121, 297
Elmegreen, B. G. & Elmegreen, D. M. 1990, ApJ, 355, 52
Elmegreen, B. G., Elmegreen, D. M., & Hirst, A. C. 2004, ApJ, 612, 191
Emsellem, E., Fathi, K., Wozniak, H., et al. 2006, MNRAS, 365, 367
England, M. N. 1989, ApJ, 344, 669
Erwin, P. 2005, MNRAS, 364, 283
Eskridge, P. B., Frogel, J. A., Pogge, R. W., et al. 2000, AJ, 119, 536
Fasano, G., Amico, P., Bertola, F., Vio, R., & Zeilinger, W. W. 1993, MNRAS, 262, 109
Fathi, K., Beckman, J. E., Piñol-Ferrer, N., et al. 2009, ApJ, 704, 1657
Fathi, K., Toonen, S., Falcón-Barroso, J., et al. 2007, ApJ, 667, L137
Faure, C., Kneib, J.-P., Covone, G., et al. 2008, ApJS, 176, 19
Gabbasov, R. F., Repetto, P., & Rosado, M. 2009, ApJ, 702, 392
Gadotti, D. A. 2008, MNRAS, 384, 420
Gadotti, D. A. 2011, MNRAS, 415, 3308
Hernandez, O., Wozniak, H., Carignan, C., et al. 2005, ApJ, 632, 253
Hoyle, B., Masters, K. L., Nichol, R. C., et al. 2011, MNRAS, 415, 3627
Hunter, Jr., J. H., England, M. N., Gottesman, S. T., Ball, R., & Huntley, J. M. 1988, ApJ, 324, 721
Ilbert, O., Arnouts, S., McCracken, H. J., et al. 2006, A&A, 457, 841
Jedrzejewski, R. I. 1987, MNRAS, 226, 747
Jogee, S., Barazza, F. D., Rix, H.-W., et al. 2004, ApJ, 615, L105
Knapen, J. H., Shlosman, I., & Peletier, R. F. 2000, ApJ, 529, 93
Koekemoer, A. M., Aussel, H., Calzetti, D., et al. 2007, ApJS, 172, 196
Kormendy, J. 1979, ApJ, 227, 714
Kormendy, J. & Kennicutt, Jr., R. C. 2004, ARA&A, 42, 603
Laine, S., Shlosman, I., & Heller, C. H. 1998, MNRAS, 297, 1052
Laine, S., Shlosman, I., Knapen, J. H., & Peletier, R. F. 2002, ApJ, 567, 97
Laurikainen, E., Salo, H., & Buta, R. 2005, MNRAS, 362, 1319
Laurikainen, E., Salo, H., Buta, R., & Knapen, J. H. 2007, MNRAS, 381, 401
Li, C., Gadotti, D. A., Mao, S., & Kauffmann, G. 2009, MNRAS, 397, 726

Lilly, S. J., Le Fèvre, O., Renzini, A., et al. 2007, ApJS, 172, 70
Lindblad, P. A. B., Lindblad, P. O., & Athanassoula, E. 1996, A&A, 313, 65
Maciejewski, W. 2006, MNRAS, 371, 451
Marinova, I. & Jogee, S. 2007, ApJ, 659, 1176
Martin, P. 1995, AJ, 109, 2428
Martinet, L. & Friedli, D. 1997, A&A, 323, 363
Martinez-Valpuesta, I., Shlosman, I., & Heller, C. 2006, ApJ, 637, 214
Masters, K. L., Nichol, R. C., Hoyle, B., et al. 2011, MNRAS, 411, 2026
Meidt, S. E., Rand, R. J., & Merrifield, M. R. 2009, ApJ, 702, 277
Méndez-Abreu, J., Corsini, E. M., Debattista, V. P., et al. 2008, ApJ, 679, L73
Méndez-Abreu, J., Sánchez-Janssen, R., & Aguerri, J. A. L. 2010, ApJ, 711, L61
Menéndez-Delmestre, K., Sheth, K., Schinnerer, E., Jarrett, T. H., & Scoville, N. Z. 2007, ApJ, 657, 790
Merrifield, M. R. & Kuijken, K. 1995, MNRAS, 274, 933
Michel-Dansac, L. & Wozniak, H. 2006, A&A, 452, 97
Mobasher, B., Capak, P., Scoville, N. Z., et al. 2007, ApJS, 172, 117
Nair, P. B. & Abraham, R. G. 2010, ApJ, 714, L260
Ohta, K., Hamabe, M., & Wakamatsu, K.-I. 1990, ApJ, 357, 71
Pérez, I., Fux, R., & Freeman, K. 2004, A&A, 424, 799
Pérez, I., Márquez, I., Freeman, K., & Fux, R. 2005, A&A, 438, 127
Pérez, I., Sánchez-Blázquez, P., & Zurita, A. 2009, A&A, 495, 775
Pfenniger, D. & Friedli, D. 1991, A&A, 252, 75
Pfenniger, D. & Norman, C. 1990, ApJ, 363, 391
Prieto, M., Aguerri, J. A. L., Varela, A. M., & Muñoz-Tuñón, C. 2001, A&A, 367, 405
Prieto, M., Gottesman, S. T., Aguerri, J.-A. L., & Varela, A.-M. 1997, AJ, 114, 1413
Puerari, I. & Dottori, H. 1997, ApJ, 476, L73+
Quillen, A. C., Frogel, J. A., & Gonzalez, R. A. 1994, ApJ, 437, 162
Rand, R. J. & Wallin, J. F. 2004, ApJ, 614, 142
Rautiainen, P., Salo, H., & Laurikainen, E. 2005, ApJ, 631, L129
Reese, A. S., Williams, T. B., Sellwood, J. A., Barnes, E. I., & Powell, B. A. 2007, AJ, 133, 2846
Regan, M. W. & Mulchaey, J. S. 1999, AJ, 117, 2676
Romano-Díaz, E., Shlosman, I., Heller, C., & Hoffman, Y. 2009, ApJ, 702, 1250
Ryden, B. S. 2004, ApJ, 601, 214
Sánchez-Blázquez, P., Ocvirk, P., Gibson, B. K., Pérez, I., & Peletier, R. F. 2011, MNRAS, 415, 709
Schwarz, M. P. 1981, ApJ, 247, 77
Schwarz, M. P. 1984a, MNRAS, 209, 93
Schwarz, M. P. 1984b, A&A, 133, 222
Scoville, N., Aussel, H., Brusa, M., et al. 2007, ApJS, 172, 1
Sellwood, J. A. 1981, A&A, 99, 362
Sellwood, J. A. & Debattista, V. P. 2006, ApJ, 639, 868
Sellwood, J. A. & Wilkinson, A. 1993, Reports on Progress in Physics, 56, 173
Sheth, K., Elmegreen, D. M., Elmegreen, B. G., et al. 2008, ApJ, 675, 1141
Sheth, K., Regan, M. W., Scoville, N. Z., & Strubbe, L. E. 2003, ApJ, 592, L13
Shlosman, I., Frank, J., & Begelman, M. C. 1989, Nature, 338, 45
Tremaine, S. & Weinberg, M. D. 1984, ApJ, 282, L5
van den Bergh, S. 2002, AJ, 124, 782
Villa-Vargas, J., Shlosman, I., & Heller, C. 2010, ApJ, 719, 1470
Weinberg, M. D. 1985, MNRAS, 213, 451
Weiner, B. J., Sellwood, J. A., & Williams, T. B. 2001, ApJ, 546, 931
Weinzirl, T., Jogee, S., Khochfar, S., Burkert, A., & Kormendy, J. 2009, ApJ, 696, 411
Whyte, L. F., Abraham, R. G., Merrifield, M. R., et al. 2002, MNRAS, 336, 1281
Wozniak, H., Friedli, D., Martinet, L., Martin, P., & Bratschi, P. 1995, A&AS, 111, 115
Zánmar Sánchez, R., Sellwood, J. A., Weiner, B. J., & Williams, T. B. 2008, ApJ, 674, 797
Zhang, X. & Buta, R. J. 2007, AJ, 133, 2584
Zimmer, P., Rand, R. J., & McGraw, J. T. 2004, ApJ, 607, 285

Appendix A: Sample galaxies

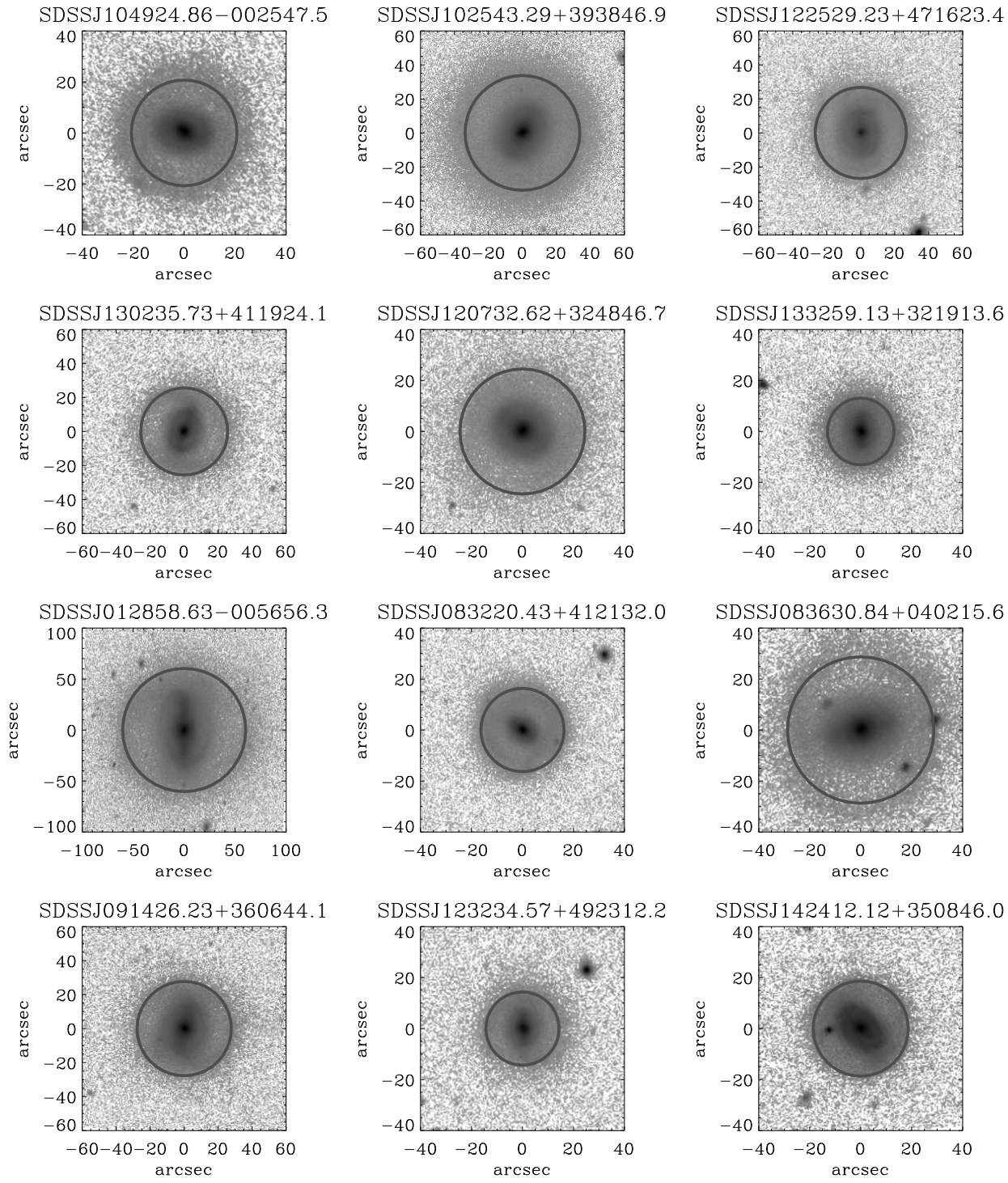

Fig. A.1: Low redshift sample with black solid circles indicating the ring size.

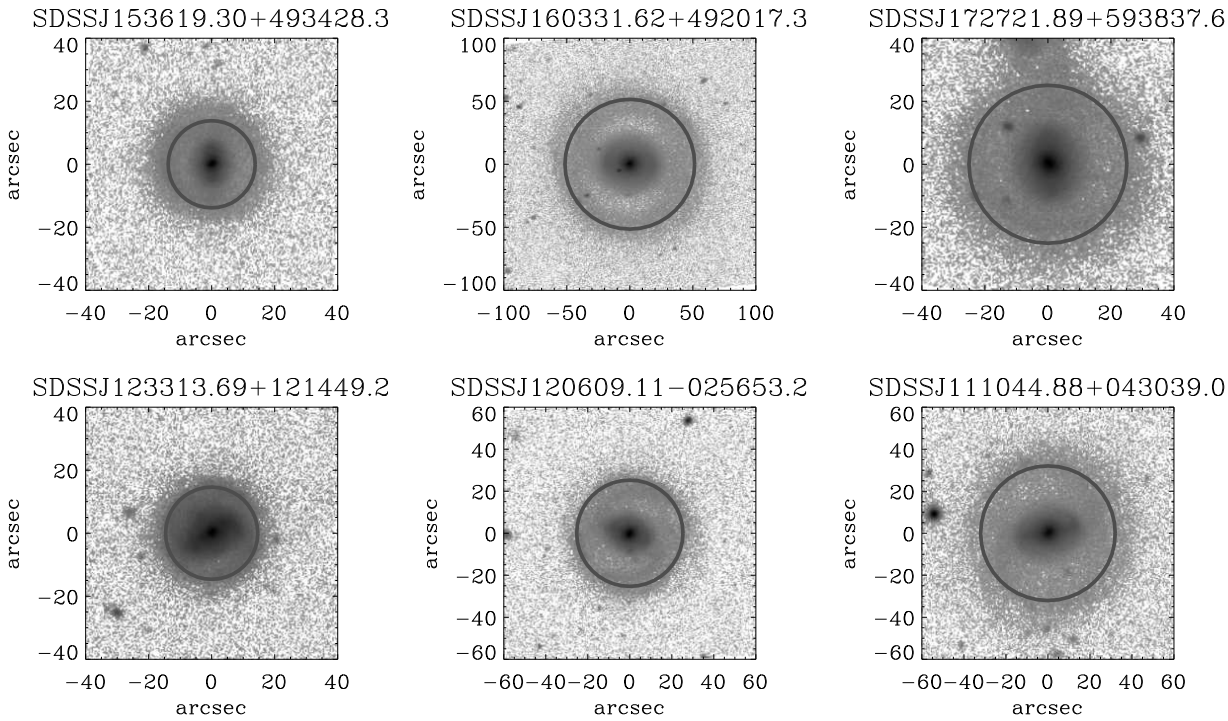

Fig. A.1: Low redshift sample with black solid circles indicating the ring size.

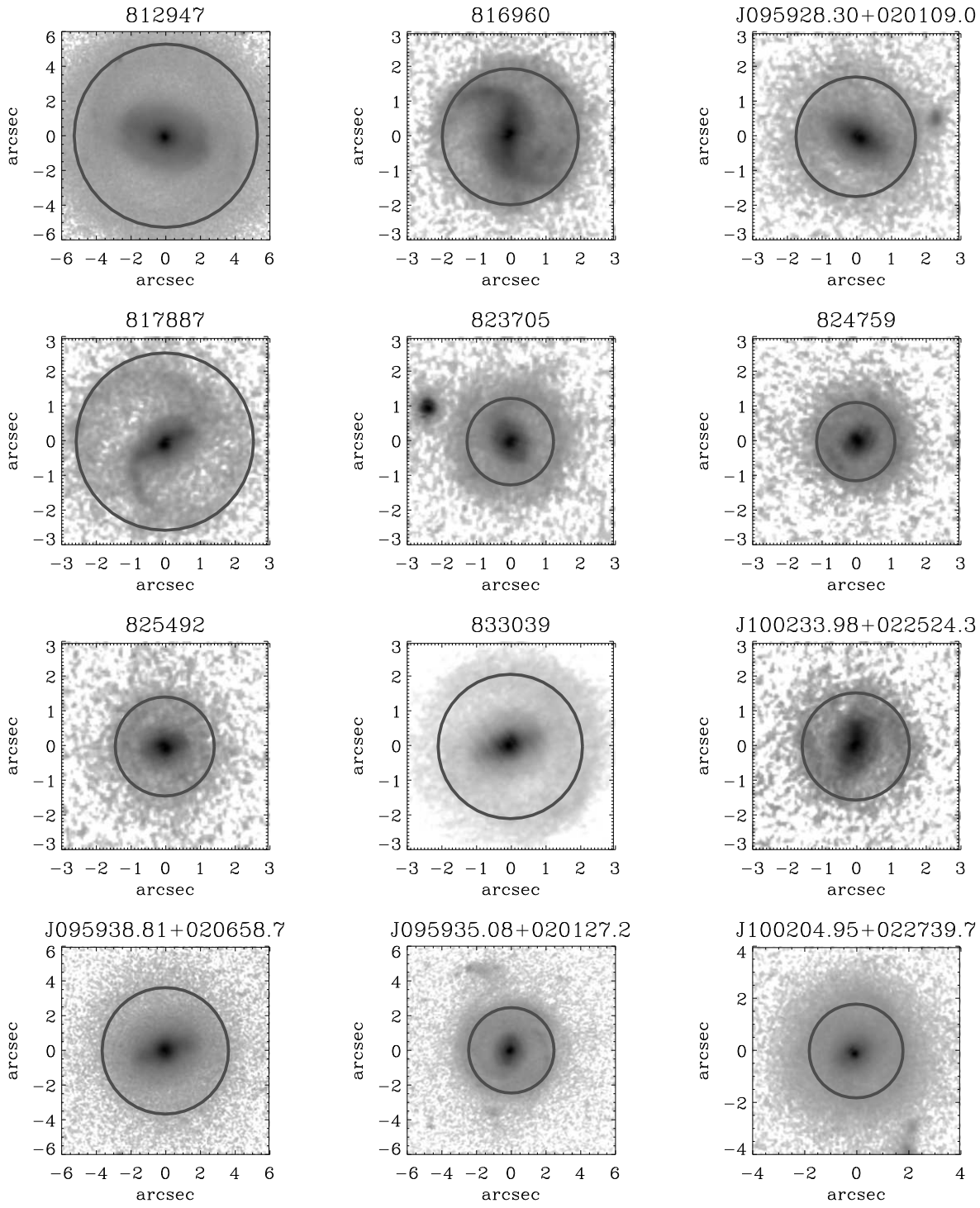

Fig. A.2: High redshift sample with black solid circles indicating the ring size.

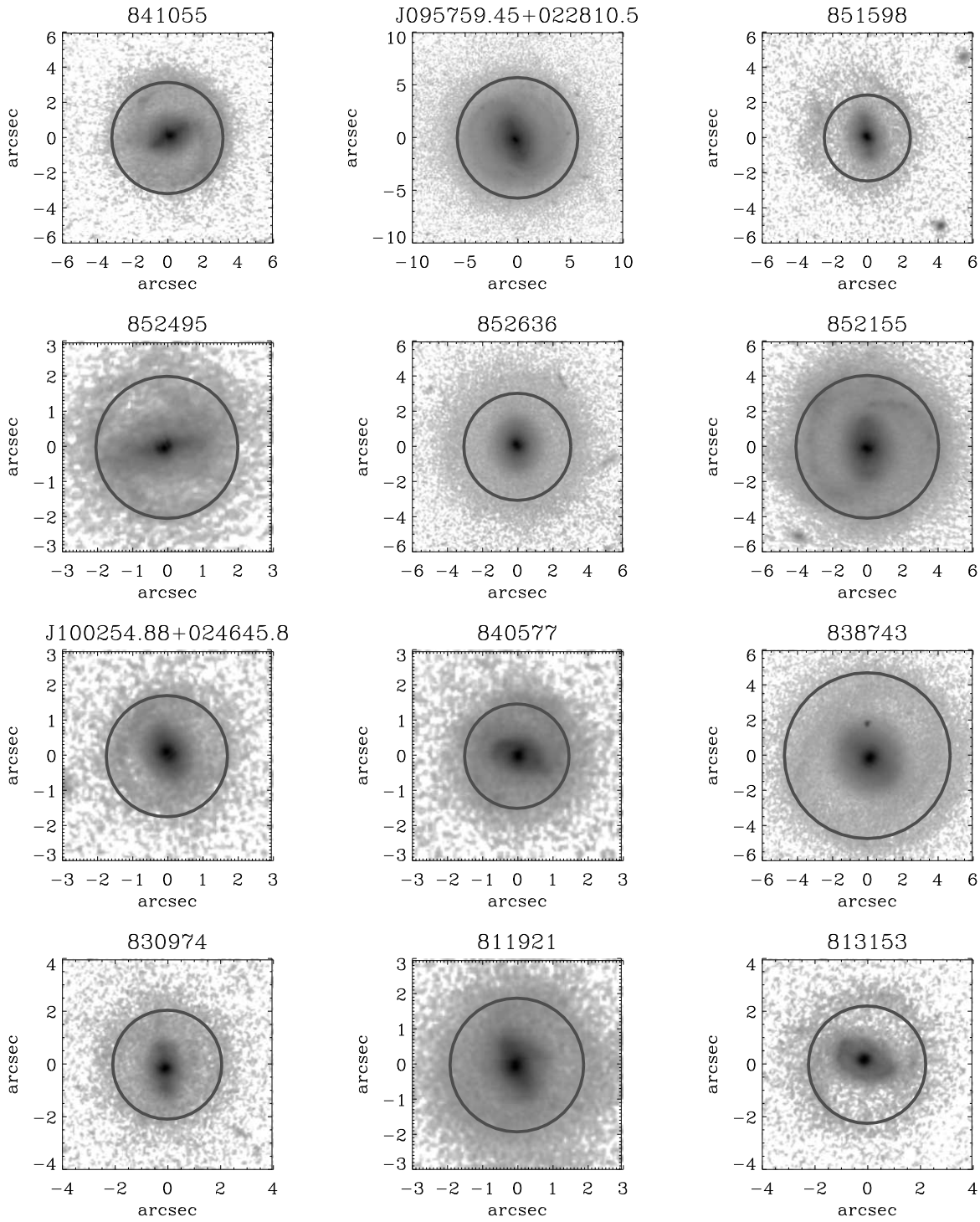

Fig. A.2: High redshift sample with black solid circles indicating the ring size.

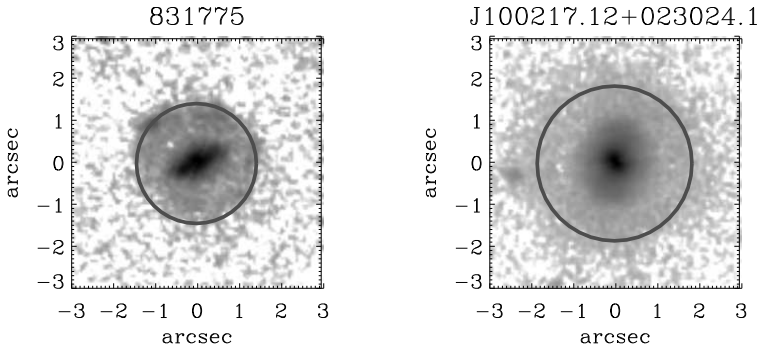

Fig. A.2: High redshift sample with black solid circles indicating the ring size.

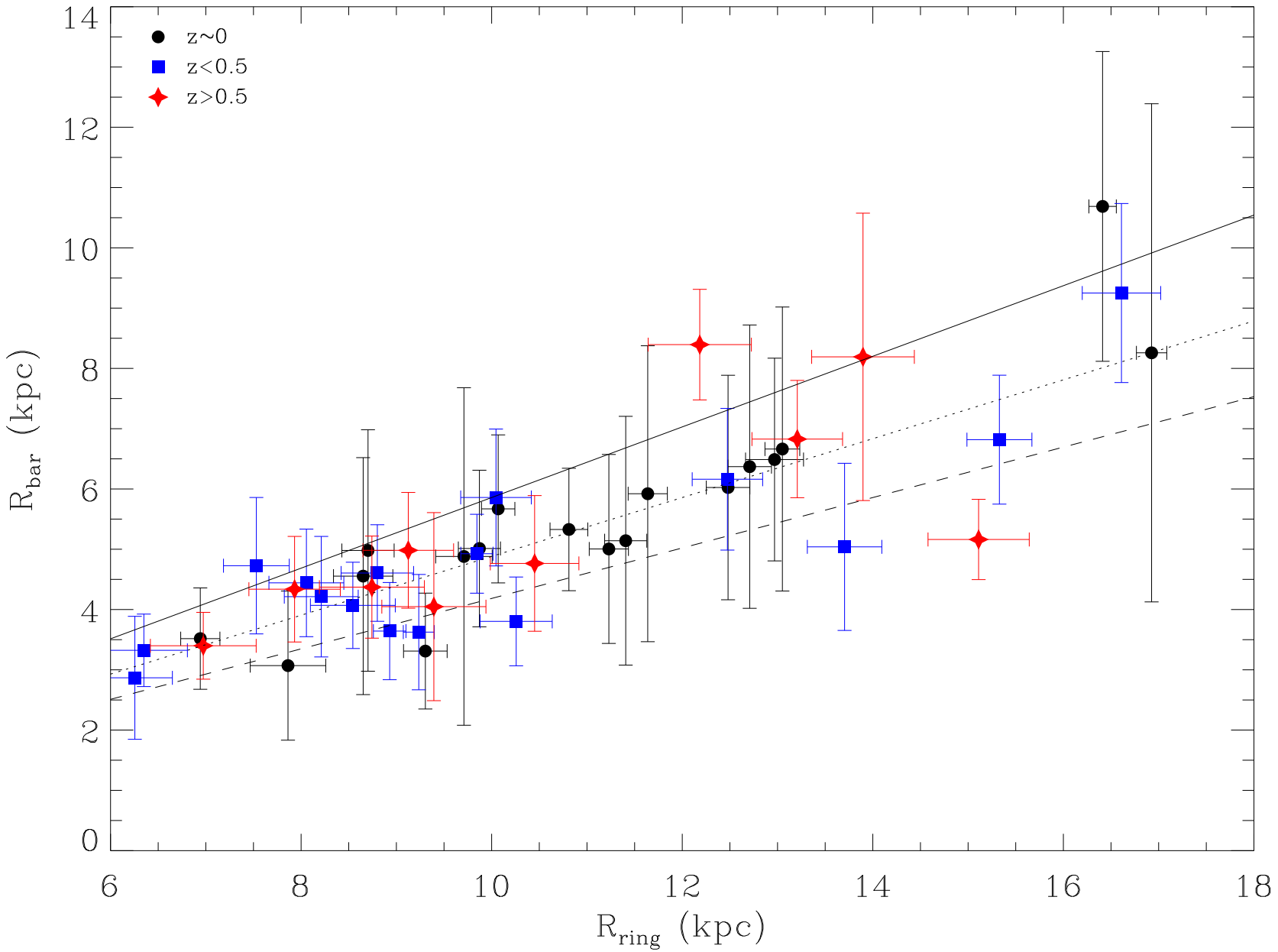
z~0
z<0.5
z>0.5
R_bar (kpc)
R_ring (kpc)
0
2
4
6
8
10
12
14
6
8
10
12
14
16
18